ACS OMEGA

http://pubs.acs.org/journal/acsodf

Article

Subunit Flexibility of Multimeric von Willebrand Factor/Factor VIII Complexes

Ernest T. Parker, Sandra L. Haberichter, and Pete Lollar*

Cite This: *ACS Omega* 2022, 7, 31183−31196

Read Online

ACCESS | Metrics & More | Article Recommendations | Supporting Information

ABSTRACT: Von Willebrand factor (VWF) is a plasma glycoprotein that participates in platelet adhesion and aggregation and serves as a carrier for blood coagulation factor VIII (fVIII). Plasma VWF consists of a population of multimers that range in molecular weight from ∼ 0.55 MDa to greater than 10 MDa. The VWF multimer consists of a variable number of concatenated disulfide-linked ∼275 kDa subunits. We fractionated plasma-derived human VWF/fVIII complexes by size-exclusion chromatography at a pH of 7.4 and subjected them to analysis by sodium dodecyl sulfate agarose gel electrophoresis, sedimentation velocity analytical ultracentrifugation (SV AUC), dynamic light scattering (DLS), and multi-angle light scattering (MALS). Weight-average molecular weights, M_w, were independently measured by MALS and by application of the Svedberg equation to SV AUC and DLS measurements. Estimates of the Mark−Houwink−Kuhn−Sakurada exponents α_{R_g}, α_s, and α_D describing the functional relationship between the *z*-average radius of gyration, $\langle R_g \rangle_z$, weight-average sedimentation coefficient, s_w, *z*-average diffusion coefficient, D_z, and M_w were consistent with a random coil conformation of the VWF multimer. Ratios of $\langle R_g \rangle_z$ to the *z*-average hydrodynamic radius, $\langle R_h \rangle_z$, estimated by DLS, were calculated across an M_w range from 2 to 5 MDa. When compared to values calculated for a semi-flexible, wormlike chain, these ratios were consistent with a contour length over 1000-fold greater than the persistence length. These results indicate a high degree of flexibility between domains of the VWF subunit.

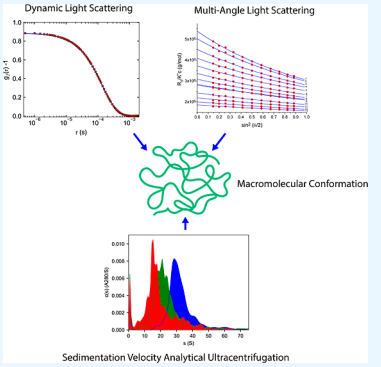

INTRODUCTION

Von Willebrand factor (VWF) is an adhesive plasma glycoprotein that is necessary for normal vertebrate hemostasis.[1−3] Following vascular injury, VWF binds to exposed subendothelial collagen in the vessel wall and mediates platelet adhesion by binding platelet glycoprotein Ibα. VWF subsequently participates in platelet aggregation by binding to platelet glycoprotein αIIbβ3.

VWF is a multimer consisting of a variable number of concatenated, ∼275 kDa subunits, called monomers. The VWF subunit propeptide contains a sequence of domains designated D1−D2−D′−D3−A1−A2−A3−D4−B1−B2−B3−C1−C2−CK. The propeptide is cleaved between the D2 and D′ domains to produce the mature D′−D3−A1−A2−A3−D4−B1−B2−B3−C1−C2−CK subunit. Subunits are disulfide-linked at their C-terminal ends to form dimers, which in turn are disulfide-linked at their N-terminal ends to form multimers.[1] VWF contains 19% carbohydrate by mass,[4] which includes extensive O-glycosylation, primarily at inter-domain segments at the N- and C-terminal ends of the A1 domain.[5] X-ray structures are available for the D′D3, A1, A2, and A3 domains and reveal that they are globular, ∼30−40 kDa proteins.[6−9]

Molecular weight estimates of plasma VWF by sodium dodecyl sulfate (SDS) agarose gel electrophoresis indicate that most multimers are distributed within a range of 1−10 MDa,[10] making VWF the largest known soluble vertebrate protein. VWF is synthesized in endothelial cells as a much larger multimer containing an estimated 3500 subunits.[2] It is either secreted constitutively or stored intracellularly as the major constituent of Weibel−Palade bodies and secreted in response to a variety of secretagogues.[11] Following secretion, VWF undergoes limited proteolysis at Tyr1605-Met1606 in the A2 domain, catalyzed by the metalloprotease ADAMTS13 to produce the molecular weight distribution found in plasma.

Congenital deficiency of VWF produces the bleeding disorder von Willebrand disease (VWD). Type I VWD, due to partial quantitative deficiency of VWF, is the most common congenital human bleeding disorder. Type II VWD is a heterogeneous group of disorders characterized by deficiency of the largest multimers. Type III VWD is due to complete absence of VWF. It is the least common type of VWD and is characterized by a severe bleeding diathesis. Deficiency of ADAMTS13 due to the congenital absence or the presence of

Received: May 31, 2022
Accepted: August 10, 2022
Published: August 25, 2022

https://doi.org/10.1021/acsomega.2c03389
ACS Omega 2022, 7, 31183−31196

autoantibodies leads to the inability to cleave VWF to lower-molecular-weight multimers. The resulting "ultra-large" VWF multimers produce the disorder thrombocytopenic thrombotic purpura.[12,13]

VWF also serves as a carrier protein for blood coagulation factor VIII (fVIII) in plasma. FVIII is a glycoprotein that functions in the activated form as a cofactor for factor IXa in the activation of factor X along the intrinsic pathway of blood coagulation. Congenital deficiency of fVIII produces the bleeding disorder hemophilia A, which is the most common severe congenital bleeding disorder. Due to variable proteolytic intracellular processing, fVIII circulates with a molecular weight that ranges from ∼160 to 240 kDa. FVIII binds tightly and non-covalently to VWF, which shields it from clearance receptors and increases its circulatory lifetime. The increased clearance rate of fVIII in type III VWD produces FVIII deficiency.

The standard model of VWF function is that under static, non-flowing conditions, attractive inter-subunit forces produce a conformation described as a "ball-of-yarn",[14] "tangled coil",[15] "compact fuzz ball",[16] "compact, bird's nest",[17] "dense globule",[18] or "compact and globular" protein.[19] According to the model, these forces are disrupted in the shear flow of the arterial circulation, leading to an elongated, active conformation that mediates the interactions of VWF with the vessel wall and platelets.

The physical characterization of size-fractionated homologous polymers is a time-honored method to characterize the macromolecular conformation.[20−22] It has been applied extensively to the characterization of synthetic polymers, polysaccharides, and nucleic acids.[23,24] As an unusual, naturally occurring homologous series of polymers, VWF lends itself to analysis using the powerful tools of polymer chemistry. We recently reported the results of sedimentation velocity analytical ultracentrifugation (SV AUC) and dynamic light scattering (DLS) studies of VWF/fVIII complexes that were fractionated by size-exclusion chromatography (SEC).[25] Molecular weights were calculated using the Svedberg equation from sedimentation coefficients and diffusion coefficients obtained by SV AUC and DLS, respectively. Conformation plots of sedimentation coefficients or diffusion coefficients versus molecular weights were consistent with a random coil conformation instead of a compact, globular structure.

By providing estimates of the radius of gyration and molecular weight, multi-angle light scattering (MALS) is an additional method by which to assess the macromolecular conformation. The ratio of the radius of gyration to the hydrodynamic radius obtained from DLS measurements provides an estimate of persistence length relative to contour length as a measure of the stiffness of a macromolecular chain.[24] In this report, we find that the persistence length is considerably shorter than the contour length of the VWF subunit, consistent with a high degree of intra-subunit flexibility.

MATERIALS AND METHODS

Alphanate (antihemophilic factor/VWF complex [human]) was purchased from Grifols USA. The native conformation of VWF/fVIII is retained in Alphanate, as judged by in vitro bioassays, the multimeric composition, clinical pharmacokinetics, and the efficacy in treating bleeding episodes in VWD and hemophilia A.[26,27] Lyophilized bovine serum albumin, fraction V RIA ELISA grade (BSA), was purchased from Calbiochem and dialyzed against 154 mM NaCl, 5.60 mM Na_2HPO_4, 1.1 mM KH_2PO_4, pH 7.40 before use as an isotropic scatterer in SEC MALS. Pooled citrated normal human plasma (FACT) was obtained from George King Biomedical. Sephacryl S-1000 was purchased from Pharmacia. An estimate of 277 kDa for the VWF subunit molecular weight was obtained from the polypeptide molecular weight of 225,388 Da and a fractional carbohydrate composition of 0.187.[4,5] The polypeptide extinction coefficient at 280 nm,[28] partial specific volume,[29] and dn/dc[30] were estimated from the amino acid composition using SEDFIT version 16.36 (www.analyticalultracentrifugation.com). Corresponding values for the glycoprotein were estimated from the fractional carbohydrate composition using 0.622 mL/g and 0.15 mL/g values for the partial specific volume[31] and dn/dc[32] of the carbohydrate, respectively. This resulted in an extinction coefficient at 280 nm of 0.65 $(mg/mL)^{-1}$ cm^{-1}, a partial specific volume of 0.706 mL/g, and a dn/dc of 0.180 mL/g for VWF. The solvent density and viscosity of 0.15 M NaCl, 0.02 M Hepes, 5 mM $CaCl_2$, pH 7.4 (HBS/Ca buffer, I 0.17) at 20 °C were measured using a DMA4500 density meter and a Lovis 2000 M rolling ball viscometer (Anton Paar USA).

Sephacryl S-1000 Size-Exclusion Chromatography. The VWF/fVIII complex was purified from Alphanate, which is a commercial product prepared from pooled human plasma by cryoprecipitation, fractional solubilization, and heparin Sepharose affinity chromatography. Human albumin is added as a stabilizer. Two vials of Alphanate were dissolved by adding 10 mL of sterile water for injection to each vial, resulting in a final volume of 21.6 mL and fVIII and VWF ristocetin cofactor activities of 180 and 250 U/mL, respectively. The sample was applied to a 2.5 × 120 cm Sephacryl S-1000 SEC column equilibrated in HBS/Ca buffer at room temperature. The column was eluted in HBS/Ca buffer at a flow rate of 0.35 mL/min controlled using a Mariotte flask, and 3.15 mL fractions were collected. The optical density of the fractions was measured at 280 and 320 nm, and the absorbance at 280 nm was corrected for light scattering by subtracting 1.7 times the OD320 from the OD280.[28] Factor VIII coagulant activity was measured using a one-stage coagulation assay using a Diagnostica Stago STart viscosity-based coagulation analyzer and referenced to pooled normal human plasma as described.[33] Thirteen samples were taken from across the VWF/fVIII peak, diluted to 0.15 mg/mL in HBS/Ca buffer, and frozen in 0.45 mL aliquots at −80 °C.

SDS/Agarose Gel Electrophoresis. Samples 1 through 13 were subjected to 0.1% lithium dodecyl sulfate/0.65% agarose gel electrophoresis and immunoblotting as described previously.[34] After the electrophoresis step, the gel was electroblotted to a nitrocellulose membrane, followed by incubation with an anti-VWF polyclonal antibody (Dako) and goat anti−rabbit IgG horse radish peroxidase (Thermo Scientific). Bands were visualized using an Amersham Imager 600 imaging system. Normal human plasma and type 2B VBD plasma served as controls.

Size-Exclusion Chromatography Multi-Angle Light Scattering. The SEC MALS configuration consisted of an isocratic pump/vial sampler/variable wavelength 1 cm path length detector (1260 Infinity II HPLC system, Agilent Corporation) in line with a Superdex 200 10/300 GL SEC column (GE Healthcare Life Sciences), a DAWN MALS detector, and an Optilab differential refractometer (Wyatt Corporation). Samples 1−13 of Sephacryl S-1000 -fractionated

https://doi.org/10.1021/acsomega.2c03389
ACS Omega 2022, 7, 31183−31196

VWF/fVIII complexes, 0.15 mg/mL, were thawed in a 37 °C water bath for 15 min, transferred to 1.5 mL bullet tubes, centrifuged at 18,000*g* for 30 min at room temperature, and transferred to 300 μL glass insert vials (Agilent). Samples (0.1 mL) were applied to the SEC column at 0.5 mL/min at room temperature. High-performance liquid chromatography (HPLC) control, data acquisition, and analysis were performed using ASTRA (version 7.3.2.21) and HPLC Manager (version 1.4.1.1) (Wyatt Corporation). In aqueous solvents, DAWN measures scattering of vertically polarized 658.3 nm GeAs laser light at 17 angles ranging from 28 to 147°. Voltage signals from 0.5 s "slices" of the chromatogram were converted to Rayleigh ratios, R_θ, by calibrating 90° light scattering with toluene[35,36] according to the instructions provided by the manufacturer. Normalization of the scattering at the other angles to the signal at 90° was performed using BSA as an isotropic scatterer. Normalization, peak alignment, and correction for band broadening were performed using ASTRA. In sufficiently dilute solution and small scattering angles (ref 37, p 305)

$$\frac{K^*c}{R_\theta} = \frac{1}{M_w}\left(1 + \frac{16\pi^2}{3\lambda_o^2}\langle R_g^2\rangle_z \sin^2\frac{\theta}{2}\right) \quad (1)$$

where M_w is the weight-average molar mass, $\langle R_g\rangle_z$ is the *z*-average radius of gyration (root mean square radius), θ is the scattering angle, c is the concentration, and λ_o is the wavelength of incident light in vacuo. K^* is an optical constant defined as follows

$$K^* = \frac{4\pi^2 n_o^2 (dn/dc)^2}{\lambda_o^4 N_A} \quad (2)$$

where n_o is the refractive index of the pure solvent, n is the refractive index of the solution containing the macromolecule, dn/dc is the macromolecular refractive index increment, and N_A is Avogadro's number. The concentration was measured using

$$\mathrm{dRI} = n - n_o = \left(\frac{dn}{dc}\right)c \quad (3)$$

where dRI is the differential refractive index.

Estimates of M_w and $(R_g)_z$ were obtained in ASTRA using the Berry[38,39] and Zimm[35,39,40] models by simple linear regression of $\sqrt{K^*c/R_\theta}$ or K^*c/R_θ versus $\sin^2(\theta/2)$, respectively.

In the limit the macromolecular concentration approaches zero (ref 37, p 304)

$$\frac{R_\theta}{K^*c} = MP(\theta) \quad (4)$$

where $P(\theta)$ is the form factor of the macromolecule. For a random coil, (ref 37, p 311; ref 41)

$$P(\theta) = (2/w^2)(e^{-w} + w - 1) \quad (5)$$

where

$$w = \frac{16\pi^2}{\lambda^2}R_g^2\sin^2\frac{\theta}{2} \quad (6)$$

substituting into eq 4 gives

$$\frac{R_\theta}{K^*c} = M(2/w^2)(e^{-w} + w - 1) \quad (7)$$

Nonlinear least-squares regression of R_θ/K^*c versus $\sin^2\theta/2$ in eq 7 was performed using ASTRA using R_G and M as the fitted parameters.

Light scattering data at both lower and higher angles can produce systematic errors in the estimated parameters.[39] High-molecular-weight impurities present in the scattering cell arising from the sample or HPLC system (e.g., shedding of SEC resin particles) contribute more to scattered light intensity at lower angles than at higher angles. Conversely, data at higher angles become increasingly distant from the extrapolation to zero angle performed by simple linear regression. Preliminary analysis of Berry plots using all 17 angles was performed to identify the range of angles that produced the optimum value of the coefficient of determination, r^2, from linear least-squares regression (Figure S1 in the Supporting Information). Data from 11 angles, 50, 57, 64, 72, 81, 90, 99, 108, 117, 126, and 134°, were selected for the final analysis. Analysis using the Zimm model produced similar results (data not shown). M_w and $(R_g)_z$ values for the entire sample were obtained from slices collected between 13.9 and 16.7 min in the Superdex 200 chromatogram using ASTRA.

Sedimentation Velocity Analytical Ultracentrifugation. VWF/fVIII S-1000 frozen aliquots, 0.15 mg/mL, were thawed in a 37 °C water bath for 15 min. SV AUC was conducted at a nominal temperature of 20 °C in a Beckman Coulter XLI analytical ultracentrifuge using standard procedures.[42] Samples (0.4 mL) were loaded into 1.2 cm pathlength Epon double sector cells equipped with sapphire windows with matched buffer in the reference sector. A small correction for temperature was performed by direct measurement of the rotor temperature, as described.[43] Data were corrected for scan time errors using REDATE version 1.01.[44] Absorbance scans at 280 nm were initiated after reaching the target rotor speeds. Data were analyzed using the continuous $c(s)$ distribution model[45−47] in SEDFIT as described previously.[25] The $c(s)$ distribution was discretized into 100 intervals over a range of 0−80 S. The fitted parameters were f/f_o, $c(s)$, time-invariant noise, and the meniscus position. Fitting was performed using sequential simplex and Marquardt−Levenberg algorithms and maximum entropy regularization with a confidence interval of 0.68. SV graphs were plotted using GUSSI version 1.2.1.[48]

The weight-average sedimentation coefficient, s_w, is given by

$$s_w = \sum_k c_k s_k / \sum_k c_k \quad (8)$$

where c_k and s_k are the total cell concentration and sedimentation coefficient of species k, respectively.[49,50] s_w values were estimated by integrating $c(s)$ distributions from 5 to 70 S. Sedimentation coefficients were adjusted to the standard condition of 20 °C in solvent water using

$$\frac{s_w}{(s_w)_{20,w}} = \frac{(\eta_0)_{20,w}}{\eta_0}\frac{(1 - \bar{\nu}\rho)}{(1 - \bar{\nu}\rho_{20,w})} \quad (9)$$

where the partial specific volume is assumed to be invariant with respect to solvent conditions, ρ and $\rho_{20,w}$ are the solvent density and density of water at 20 °C, respectively, and η_0 and $(\eta_0)_{20,w}$ are the corresponding solvent viscosities.[37]

Dynamic Light Scattering. VWF/fVIII S-1000 frozen aliquots, 0.15 mg/mL, were thawed in a 37 °C water bath for 15 min and centrifuged at 18,000*g* 30 min in a Beckman Microfuge 18 centrifuge. The upper 0.4 mL volume was

https://doi.org/10.1021/acsomega.2c03389
ACS Omega 2022, 7, 31183−31196

removed and added to a fresh 1.5 mL bullet tube. Measurements of the normalized intensity autocorrelation function, $g_2(\tau)$, as a function of decay time, τ, were carried out on 0.02 mL samples at 20 °C in a 3 mm ZEN2112 quartz cuvette using a Zetasizer Nano S system (Malvern Panalytical) at a scattering angle of 175° using a 633 nm He Ne laser in the automatic attenuation mode. Four measurements were carried out on each sample in situ. The procedure was repeated on the same thawed aliquots for a total of two experiments.

For a polydisperse system, the normalized field autocorrelation function, $g_1(\tau)$ is characterized by a distribution of exponential decay rates, $G(\Gamma)$, given by[51,52]

$$g_1(\tau) = \int_0^\infty G(\Gamma)\exp(-\Gamma\tau)\mathrm{d}\Gamma \tag{10}$$

The measured $g_2(\tau)$ values are related to $g_1(\tau)$ by the Siegert relationship

$$g_2(\tau) = B + \beta[g_1(\tau)]^2 \tag{11}$$

where B theoretically equals 1 but varies experimentally due to noise. β, called the coherence factor, depends on the experimental geometry.

For macromolecules sufficiently small relative to the incident wavelength of light, the decay rate is related to the translational diffusion coefficient, D, by

$$\Gamma = Dq^2 \tag{12}$$

where q is the magnitude of the scattering vector

$$q = \frac{4\pi n_o}{\lambda_o}\sin(\theta/2) \tag{13}$$

The mean $(\mu_1 = \overline{\Gamma})$ and variance (μ_2) of the $G(\Gamma)$ distributions and B and β in the Siegert relationship were estimated by fitting $g_2(\tau)$ versus τ values using the cumulant analysis model in SEDFIT, which is based on the method described by Frisken.[51,53] $\overline{\Gamma}$ is the z-average diffusion coefficient, D_z,[52]

$$D_z = \sum_k c_k m_k D_k \Big/ \sum_k c_k m_k \tag{14}$$

where c_k, m_k, and D_k are the total cell concentration, mass, and diffusion coefficient of species k, respectively.

Diffusion coefficients were adjusted to the standard condition of 20 °C in solvent water using (ref 54, p 584)

$$\frac{D}{D_{20,w}} = \frac{T}{T_{20}}\frac{\eta_{20,w}}{\eta_0} \tag{15}$$

where T and T_{20} are the absolute experimental temperature and temperature at 20 °C, respectively, and $\eta_{20,w}$ is the viscosity of water at 20 °C. The z-average diffusion coefficient under standard conditions is then $(D_z)_{20,w}$. The polydispersity index (PDI) was calculated using[55]

$$\mathrm{PDI} = \frac{\mu_2}{\overline{\Gamma}^2} \tag{16}$$

Molecular Weights, Frictional Ratios, and Hydrodynamic Radii from SV AUC and DLS Measurements. Molar masses were estimated using the Svedberg equation

$$M = \frac{sRT}{D(1-\overline{\nu}\rho)} \tag{17}$$

where R is the gas constant.[56] If the weight-average sedimentation coefficient, s_w, and z-average diffusion coefficient, D_z, are used in the Svedberg equation, then the weight-average molecular weight, M_w, is obtained.[52,57] $(s_w)_{20,w}$ and $(D_z)_{20,w}$ values were averaged for use in the calculation. No correction was performed for concentration dependence of the sedimentation coefficient.

Frictional coefficients were calculated using the Einstein diffusion equation[58,59]

$$D = \frac{RT}{N_A f} \tag{18}$$

Frictional ratios, f/f_o, were calculated using (ref 54, p 585)

$$f_0 = 6\pi\eta_0\left(\frac{3M\overline{\nu}}{4\pi N_A}\right)^{1/3} \tag{19}$$

where f_o is the frictional coefficient of the equivalent sphere having the same anhydrous molecular weight and partial specific volume, $\overline{\nu}$, of the macromolecule and M is the molar mass of the macromolecule estimated using the Svedberg equation (eq 18).

Ratios of Equivalent Radii for VWF/fVIII Complexes. The equivalent radius for a solution property, for example, translational diffusion coefficient, D, or radius of gyration, R_g, is the radius of a spherical particle having the same value of the solution property as that of the macromolecule under consideration.[60] The equivalent radius corresponding to R_g is (ref 36, p 259)

$$a_G = \sqrt{\frac{5}{3}}R_g \tag{20}$$

a_G values were calculated using the Berry model $(R_g)_z$ values for samples 1−13. The equivalent radius corresponding to D is the hydrodynamic radius, R_h, also denoted as a_T,[60] which is calculated using the Stokes−Einstein equation[58]

$$R_h = a_T = \frac{1}{6\pi\eta_0}\frac{RT}{N_A D} \tag{21}$$

a_T values were calculated using the mean $(D_z)_{20,w}$ values of samples 1−13. a_G/a_T ratios for a random coil in a good solvent and in a Θ-solvent and for wormlike chains with contour length/persistence length, L/P, ratios of 15 and 1090, respectively and a diameter of 2.1 nm were obtained from Table 1 in Garcia de la Torre and Hernández Cifre,[24] where the contour length is the largest end-to-end distance of a coil and the persistence length is the projection of the vector pointing from one end of the chain to the other onto the unit vector along the direction of the first two chain segments (ref 36, p 246). The a_G/a_T ratio of a rod corresponding to the contour length and diameter of the VWF subunit of 70 and 2.5 nm, according to electron microscopy, respectively,[16,61] and the L/d ratio of 28 were calculated using eqs 1 and 13 in Ortega and Garcia de la Torre.[62]

Statistical Analysis. The linear model of $\log_{10}\langle R_g\rangle_z$, $\log_{10}(s_w)_{20,w}$, or $\log_{10}(D_z)_{20,w}$ as the Y variable and $\log_{10} M_w$ as the X variable was fitted using orthogonal regression[63] since both variables are subject to error, assuming equal uncertainties in the variables. The 95% confidence interval of the slope of the regression line was calculated as described.[64]

https://doi.org/10.1021/acsomega.2c03389
ACS Omega 2022, 7, 31183−31196

Table 1. SEC MALS of Size-Fractionated VWF/fVIII Complexes

	M_w (MDa)			$\langle R_g \rangle_z$ (nm)		
sample	Zimm	Berry	coil	Zimm	Berry	coil
1	5.50	5.28	5.32	63.3	56.2	57.1
2	5.27	5.06	5.09	60.8	54.4	55.1
3	4.69	4.56	4.58	56.4	51.2	51.7
4	4.23	4.14	4.15	53.3	48.7	49.2
5	3.91	3.84	3.85	49.9	46.1	46.4
6	3.49	3.43	3.44	48.4	44.7	45.1
7	3.20	3.15	3.15	47.8	43.0	43.2
8	2.87	2.84	2.84	43.1	40.5	40.7
9	2.96	2.93	2.93	41.4	39.0	39.2
10	2.43	2.41	2.41	39.7	37.5	37.5
11	2.23	2.21	2.22	38.9	36.1	36.4
12	2.08	2.06	2.06	37.3	34.4	34.6
13	1.97	1.95	1.95	35.2	32.9	33.0

Calculations were performed using Prism (version 7.05). Confidence limits for D_z in Figure S2 in the Supporting Information were calculated using Student's t distribution based on four measurements on each sample in situ and thus do not account for variation due to sample thawing and preparation for DLS.

RESULTS

SEC Fractionation of VWF/fVIII Complexes. The commercial VWF/fVIII product, Alphanate, was fractionated by Sephacryl S-1000 SEC in HBS/Ca buffer at a pH of 7.4 as described in the Materials and Methods section. The absorbance at 280 nm (A280) and fVIII coagulant activity of fractions are shown in Figure 1A. Thirteen samples were taken across the fVIII peak, as shown in the figure, diluted to a concentration of 0.15 mg/mL in HBS/Ca buffer, aliquoted, and frozen at −80 °C for further analysis.

SDS agarose gel electrophoresis resolves VWF multimers into bands corresponding to individual multimers.[34] Analysis of samples 1−13 in Figure 1A with detection by Western blotting revealed fractionation of VWF into subpopulations in which most of the band intensity was present in three or four bands (Figure 1B). The bands in normal human plasma are labeled i through xii. Band i corresponds to the ∼0.55 MDa VWF dimer. Assuming that additional bands correspond to sequential addition of dimers, bands ii through xii correspond to multimers with molecular weights of 1.10, 1.65, 2.20, 2.74, 3.30, 3.85, 4.40, 4.95, 5.50, 6.05, 6.60, and 7.15 MDa, respectively.

SEC MALS of Size-Fractionated VWF/fVIII Complexes. Samples 1−13 of Sephacryl S-1000 SEC-fractionated VWF/fVIII (Figure 1A) underwent Superdex 200 SEC MALS. The rationale for additional SEC was not to achieve additional size fractionation since proteins larger than 0.6 MDa typically appear in the void volume following Superdex 200 SEC. Rather, the additional SEC step provided uniform, automated sample delivery to the absorbance and MALS detectors and differential refractometer and low background light scattering noise. Figure 2A shows 90 degree light scattering, absorbance at 280 nm, and the differential refractive index of the Superdex 200 chromatogram of sample 9. All 13 samples produced similar elution patterns and absorbance yields.

Estimates of the weight-average molecular weight, M_w, and radius of gyration $\langle R_g \rangle_z$ were obtained by simple linear

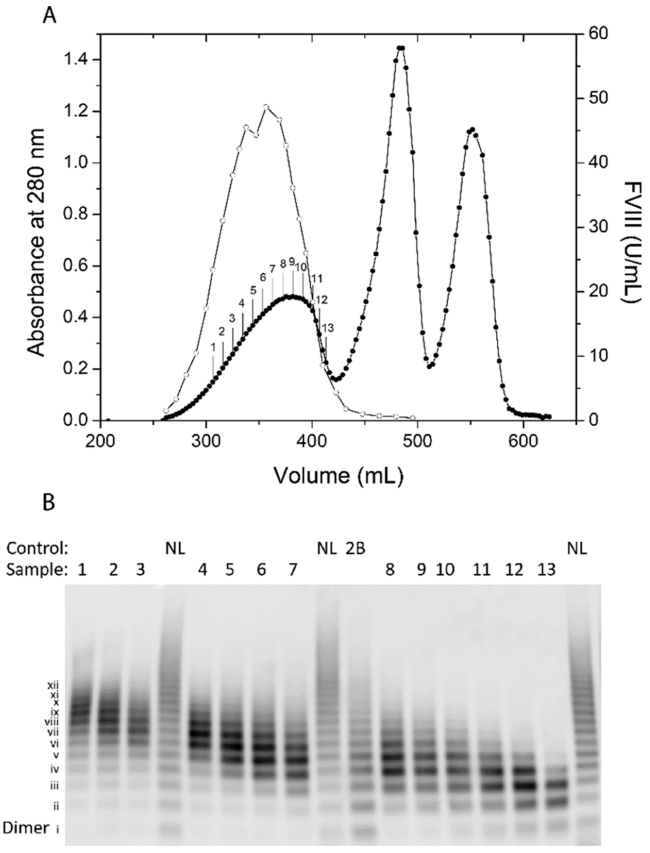

Figure 1. Sephacryl S-1000 SEC of unfractionated VWF/fVIII complexes. (A) Two vials of the commercial VWF/fVIII product, Alphanate, were reconstituted in sterile water for injection and applied to a 2.5 × 120 cm Sephacryl S-1000 column equilibrated in HBS/Ca buffer at a pH of 7.4 as described in the Materials and Methods section. Closed circles, absorbance at 280 nm; open circles, fVIII coagulant activity. Fractions across the VWF/fVIII peak, designated samples 1 through 13, were diluted to 0.15 mg/mL into HBS/Ca buffer and frozen at −80 °C. (B) SDS/agarose gel electrophoresis of samples 1 through 13. NL, normal human plasma; 2B, human type 2B VBD. The markers i to xii correspond to bands in normal human plasma.

regression using the Berry[38] and Zimm[35,40] models as described in the Materials and Methods section. Figure 2B shows the results using the Berry model for the peak maximum fractions of the Superdex 200 chromatograms. To obtain estimates of M_w and $\langle R_g \rangle_z$ for the entire sample, regression analysis from slices from 13.9 to 16.7 min in the Superdex 200 chromatograms were used (Table 1). The Zimm model produced higher estimates of $\langle R_g \rangle_z$ than the Berry model (Table 1). This difference ranged from 12% for sample 1 to 7% for sample 13. Estimates of M_w agreed to within 5% for all samples with almost negligible difference for the smallest multimers (Table 1).

SV AUC of Size-Fractionated VWF/fVIII Complexes. Samples 1 through 13 (Figure 1A) were subjected to SV AUC. Two separately thawed aliquots of each sample were run, except for sample 13, which was run only once due to insufficient material. Absorbance at 280 nm was measured as a function of time and radial position. Scans from sample 9 along with the fit to the continuous $c(s)$ distribution model in SEDFIT are shown in Figure 3A as a representative sample. Fits were obtained on the order of the random noise in the

https://doi.org/10.1021/acsomega.2c03389
ACS Omega 2022, 7, 31183−31196

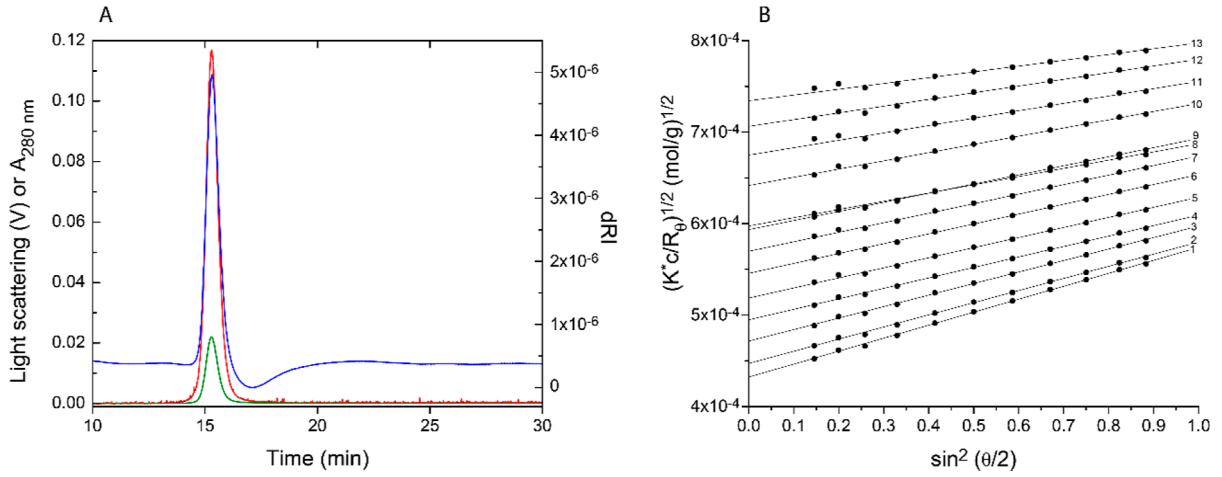

Figure 2. SEC MALS of size-fractionated VWF/fVIII complexes. Samples 1−13 of Sephacryl S-1000 -fractionated VWF/fVIII complexes (Figure 1A) were subjected to Superdex 200 SEC MALS as described in the Materials and Methods section. (A) Superdex 200 SEC of sample 9. Red, light scattering at 90°; green, absorbance at 280 nm/1 cm pathlength; and blue, differential refractive index. (B) Berry plots. Rayleigh ratios, R_θ, and macromolecular concentrations, c, were measured from scattered light intensities and differential refractive indices of Superdex 200 SEC slices at the peak maxima for samples 1−13, as described in the Materials and Methods section. K^*, optical constant (eq 1). Lines, simple linear regression fits.

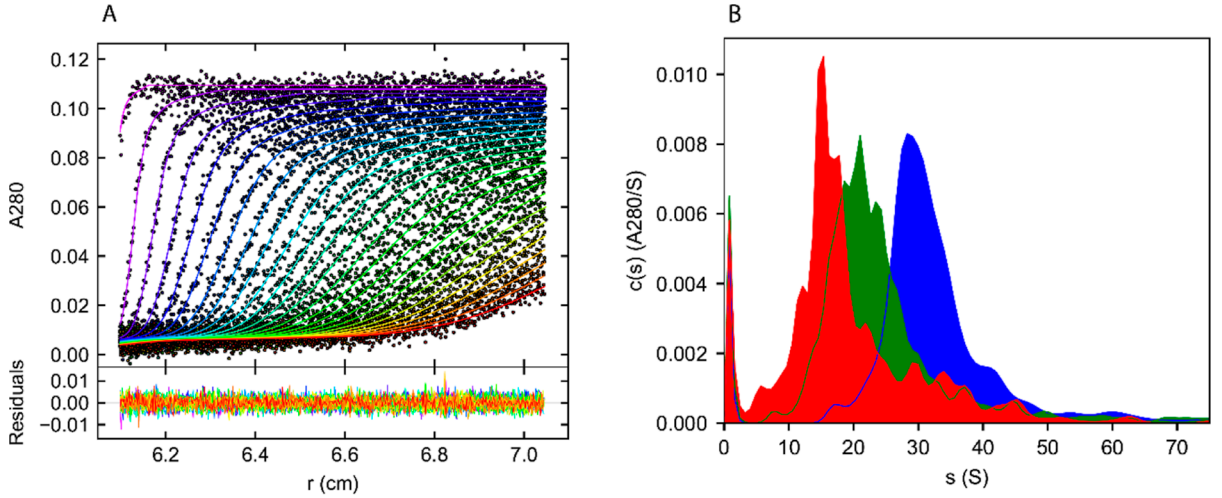

Figure 3. SV AUC of size-fractionated VWF/fVIII complexes. (A) Sephacryl S-1000 VWF/FVIII sample 9 (Figure 1A), 0.15 mg/mL in HBS/Ca buffer, was centrifuged at 45,400g in a Beckman−Coulter XLI analytical ultracentrifuge as described in the Materials and Methods section. Absorbance scans at 280 nm from left to right represent increasing times during centrifugation. Curves represent fits to the continuous c(s) distribution model in SEDFIT. (B) c(s) distributions of samples 1 (blue), 9 (green), and 13 (red).

data acquisition for all 13 samples (Table 2). The fitted peak loading concentrations were similar for all samples, indicating that there were no sample-dependent artifacts due to the freeze−thaw process (Table 2). Representative c(s) distributions shown in Figure 3B for samples 1, 9, and 13 and reveal widths indicative of polydispersity, consistent with SDS agarose gel electrophoresis (Figure 1B). The weight-average sedimentation coefficients, adjusted to the standard condition, $(s_w)_{20,w}$, of 20 °C in solvent water, of samples 1−13 were estimated by integration of the continuous c(s) distributions.[50,65] $(s_w)_{20,w}$ values decreased with increasing SEC elution volume, consistent with fractionation from higher to lower molecular weights (Table 2).

DLS of SEC-Fractionated VWF/fVIII Complexes. DLS measurements were obtained on samples 1−13 (Figure 1A) to obtain estimates of the z-average diffusion coefficients, adjusted to the standard condition, $(D_z)_{20,w}$, of 20 °C in solvent water, and hydrodynamic radii. Two experiments consisting of a set of four measurements were conducted on each sample. Measurements of the normalized electric intensity autocorrelation function, $g_2(\tau)$, as a function of decay times were fitted by cumulants analysis, as described in the Materials and Methods section. $(D_z)_{20,w}$ values did not vary over a concentration range from 0.02 to 0.15 mg/mL (Figure S2) and thus represent estimates of the values at infinite dilution, $(D_z^0)_{20,w}$. Only fits to samples 1, 3, 5, 7, 9, 11, and 13 are shown for clarity (Figure 4). The decay curves shift from right to left from samples 1 to 13, respectively, corresponding to increasing SEC elution volume, consistent with faster diffusion and smaller hydrodynamic radii of the eluting species. $(D_z)_{20,w}$ values, obtained from the first moment of the cumulants analysis, ranged from 0.595×10^{-7} to 0.961×10^{-7} cm^2 s^{-1} (Table 3). The PDIs obtained from the second moment of the

https://doi.org/10.1021/acsomega.2c03389
ACS Omega 2022, 7, 31183−31196

Table 2. SV AUC of Size-Fractionated VWF/fVIII Complexes[a]

experiment	1			2		
Ssample	$(s_w)_{20,w}$ (S)	signal	rmsd	$(s_w)_{20,w}$ (S)	signal	rmsd
1	33.47	0.100	0.0041	34.74	0.104	0.0025
2	31.63	0.103	0.0037	32.39	0.103	0.0025
3	30.77	0.103	0.0035	31.45	0.093	0.0030
4	30.52	0.095	0.0033	30.10	0.102	0.0029
5	29.18	0.094	0.0039	28.97	0.100	0.0028
6	28.02	0.102	0.0035	27.39	0.110	0.0028
7	26.65	0.105	0.0032	26.50	0.119	0.0036
8	26.27	0.104	0.0030	25.43	0.119	0.0033
9	25.04	0.102	0.0024	24.72	0.117	0.0032
10	24.20	0.102	0.0024	25.01	0.115	0.0029
11	23.07	0.102	0.0027	24.09	0.111	0.0030
12	22.72	0.101	0.0032	22.50	0.113	0.0031
13	21.23	0.100	0.0027	ND	ND	ND

[a]Signal: fitted loading A_{280nm}. rmsd: root mean square deviation to the fitted $c(s)$ distribution. ND: not determined.

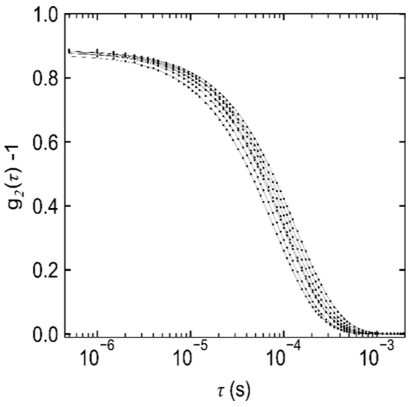

Figure 4. DLS of SEC-fractionated VWF/fVIII complexes. DLS measurements were obtained of the normalized intensity autocorrelation function, $g_2(\tau)$, on samples 1−13 of Sephacryl S-1000 -fractionated VWF/fVIII (Figure 1A) in HBS/Ca buffer, as described in the Materials and Methods section. Plots of $g_2(\tau) - 1$, vs decay time, τ, are shown for the median decay rate of four measurements of samples 1, 3, 5, 7, 9, 11, and 13, from right to left, respectively. The curves represent fits to the cumulants analysis model in SEDFIT. The first and second moments of the cumulants fit were used to calculate the z-average diffusion coefficients and PDIs given in Table 3.

cumulants analysis ranged from 0.13 to 0.21 (Table 3). Values below 0.15 are considered consistent with monodispersity.[55] Thus, the polydispersity identified by DLS is consistent with the results of SDS agarose gel electrophoresis and SV AUC (Figures 1B and 3B).

Molecular Weights, Hydrodynamic Radii, and Frictional Ratios of SEC-Fractionated VWF/fVIII Complexes Obtained from SV and DLS Measurements. M_w values for samples 1−13 (Figure 1A) were estimated using the Svedberg equation (eq 17) and the $(s_w)_{20,w}$ and $(D_z)_{20,w}$ values in Tables 2 and 3, as shown in Table 4, and ranged from 1.8 to 4.9 MDa. Hydrodynamic radii were calculated using the Stokes−Einstein equation (eq 21) and ranged from 22.4 to 37.4 nm (Table 4). Frictional ratios were estimated from the values of M_w and $(D_z)_{20,w}$ (Table 4) using the Einstein diffusion equation and the Stokes−Einstein equations (eqs 18 and 19). A frictional ratio, f/f_0, greater than unity is a measure of departure from

Table 3. DLS of Size-Fractionated VWF/fVIII Complexes[a]

experiment	1		2	
sample	$(D_z)_{20,w}$ (F)	PDI	$(D_z)_{20,w}$ (F)	PDI
1	0.575	0.202	0.572	0.217
2	0.592	0.194	0.596	0.175
3	0.614	0.192	0.615	0.191
4	0.628	0.210	0.643	0.157
5	0.669	0.150	0.672	0.140
6	0.700	0.144	0.702	0.127
7	0.719	0.138	0.720	0.126
8	0.723	0.196	0.745	0.148
9	0.759	0.177	0.772	0.151
10	0.800	0.162	0.804	0.154
11	0.833	0.172	0.849	0.150
12	0.904	0.131	0.899	0.136
13	0.953	0.208	0.961	0.187

[a]F = Fick; 1 F = 1×10^{-7} cm^2 s^{-1}. PDI: polydispersity index.

Table 4. Weight-Average Molecular Weights, Frictional Ratios, and z-Average Hydrodynamic Radii of SEC-Fractionated VWF/fVIII Complexes from SV and DLS Measurements

sample	M_w (MDa)	$(R_h)_z$ (nm)	f/f_0
1	4.91	37.4	3.36
2	4.45	36.1	3.35
3	4.18	34.9	3.31
4	3.94	33.7	3.27
5	3.58	32.0	3.20
6	3.26	30.6	3.15
7	3.06	29.8	3.14
8	2.95	29.2	3.11
9	2.70	28.0	3.08
10	2.49	26.7	3.01
11	2.26	25.5	2.97
12	2.08	23.8	2.85
13	1.83	22.4	2.80

https://doi.org/10.1021/acsomega.2c03389
ACS Omega 2022, 7, 31183−31196

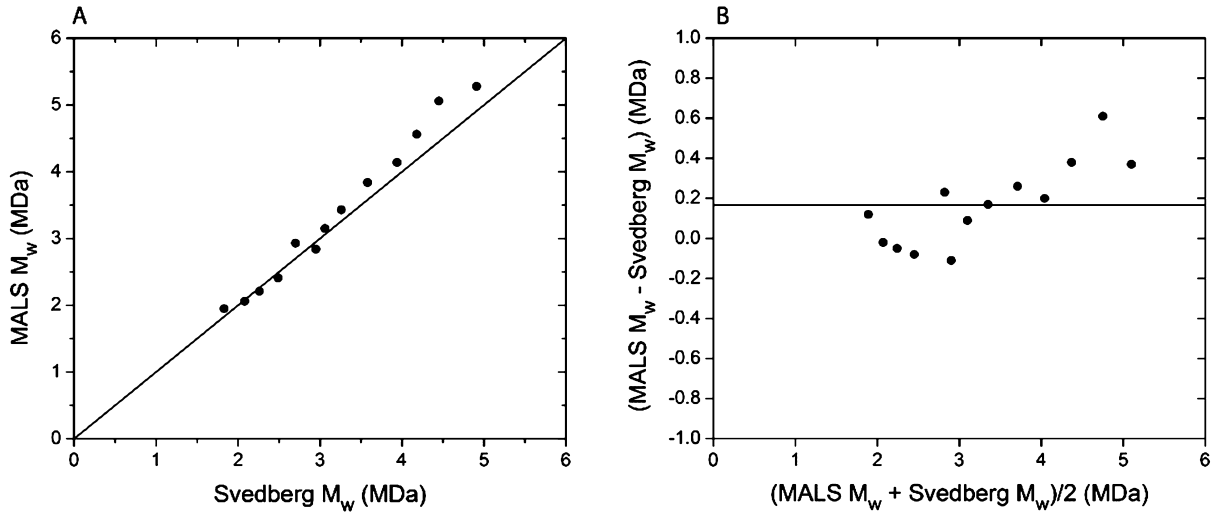

Figure 5. Comparison of molecular weights of SEC-fractionated VWF/fVIII complexes estimated by MALS and using the Svedberg equation. (A) Molecular weight estimates for samples 1−13 of Sephacryl S-1000 -fractionated VWF/fVIII (Figure 1A) were calculated using the Svedberg equation (Table 4) and are plotted vs MALS estimates using the Berry model (Table 1). Also shown is the line of unity. (B) Bland−Altman plot. The horizontal line represents the mean difference.

the spherical geometry and/or hydration of the macromolecule.[66] The large values in Table 4, which increase with increasing molecular weight, are consistent with a non-globular conformation of VWF, which becomes more pronounced as the multimer size increases.

Comparison of Molecular Weights of SEC-Fractionated VWF/fVIII Complexes Estimated by MALS and Using the Svedberg Equation. M_w values estimated by MALS using the Berry model (Table 1) and the Svedberg equation (Table 4) were compared (Figure 5A). A line of unity is drawn to show the differences between the two methods. A Bland−Altman plot[67] of the differences versus the average values is shown in Figure 5B. The mean difference/average value ratio was 4%, indicating a good agreement between the two methods. The horizontal line represents the mean difference of 0.17 MDa. The 95% confidence limits for the mean difference are 0.04 and 0.29 MDa. Equivalently, Student's *t*-test for the hypothesis of zero mean difference was rejected at the 0.05 level of significance (p = 0.015). This indicates that there is a bias in the measurements[67] and the MALS estimates are higher than the Svedberg estimates. Orthogonal regression of the scatter plot in Figure 5B revealed that the difference in the two estimates increased with molecular weight, producing a slope estimate of a 0.16 MDa difference per MDa, which was significantly greater than zero (p = 0.001). We consider the bias and molecular weight dependence of the differences small relative to the molecular weights. Because it is not possible to determine which method or both are subject to systematic error, molecular weight estimates obtained using both methods were used for subsequent analysis.

Conformation of SEC-Fractionated VWF/fVIII Complexes. Figure 6 shows the conformation plots of $\log_{10}\langle R_g\rangle_z$, $\log_{10}(s_w)_{20,w}$, and $\log_{10}(D_z)_{20,w}$ versus either MALS or Svedberg $\log_{10}$ M_w for samples 1−13 of SEC-fractionated VWF/fVIII complexes (Figure 1A). The estimates of the Mark−Houwink−Kuhn−Sakurada (MHKS) exponents α_{R_g}, α_s, and α_D obtained from the slopes of the regression lines are shown in the figure and in Table 5. There is a reasonably good agreement between MHKS exponents with M_w values estimated using MALS or the Svedberg equation. Table 6 shows the MHKS exponents expected for spheres, random coils, and rods. The sedimentation coefficients of globular proteins closely obey the α_s exponent of 0.67 predicted for spheres.[68] Exponents are listed for a random coil in the presence and absence of the excluded volume effect, which is due the inability of segments to overlap in space.[22] This increases $\langle R_g\rangle$ compared to that for a hypothetical, ideal coil in which an overlap of segments is allowed and there is no excluded volume. Segment−segment interactions can lead to partial collapse of a random coil, giving it the properties that resemble an ideal coil. The MHKS exponents are consistent with a random coil conformation intermediate between an excluded volume and a non-excluded volume conformation.

SEC MALS Random Coil Model of Size-Fractionated VWF/fVIII Complexes. Since the conformation plots were consistent with a random coil conformation for the VWF/fVIII complex (Figure 6), MALS data in Figure 2 representing Superdex 200 SEC slices at the peak maxima for samples 1−13 were replotted as R_θ/K^*c versus $\sin^2(\theta/2)$ and fit to a random coil model using M_w and $(R_g)_z$ as the fitted parameters, as described in the Materials and Methods section (Figure 7). Analysis of slices from 13.9 to 16.7 min in the Superdex 200 chromatograms was performed to obtain estimates of M_w and $\langle R_g\rangle_z$ for the entire sample. The results revealed a close agreement between the random coil and Berry models (Table 1).

Ratios of Equivalent Radii, a_G/a_T, of Size-Fractionated VWF/fVIII Complexes. The macromolecular conformation can also be assessed from the measurement of ratios of equivalent radii, a_G/a_T, where $a_G = \sqrt{5/3}R_g$ and $a_T = R_h$.[24,60] The a_G/a_T ratio for a sphere is 1. Ratios for a random coil based on rigid body Monte Carlo simulations are 1.87 and 1.65 in the presence and absence of excluded volume effects, respectively.[24,60,69−71] The a_G/a_T ratio of a rod can be calculated as function of the L/d ratio, where L and d are the contour length and diameter, respectively.[60,62] Using estimates

https://doi.org/10.1021/acsomega.2c03389
ACS Omega 2022, 7, 31183−31196

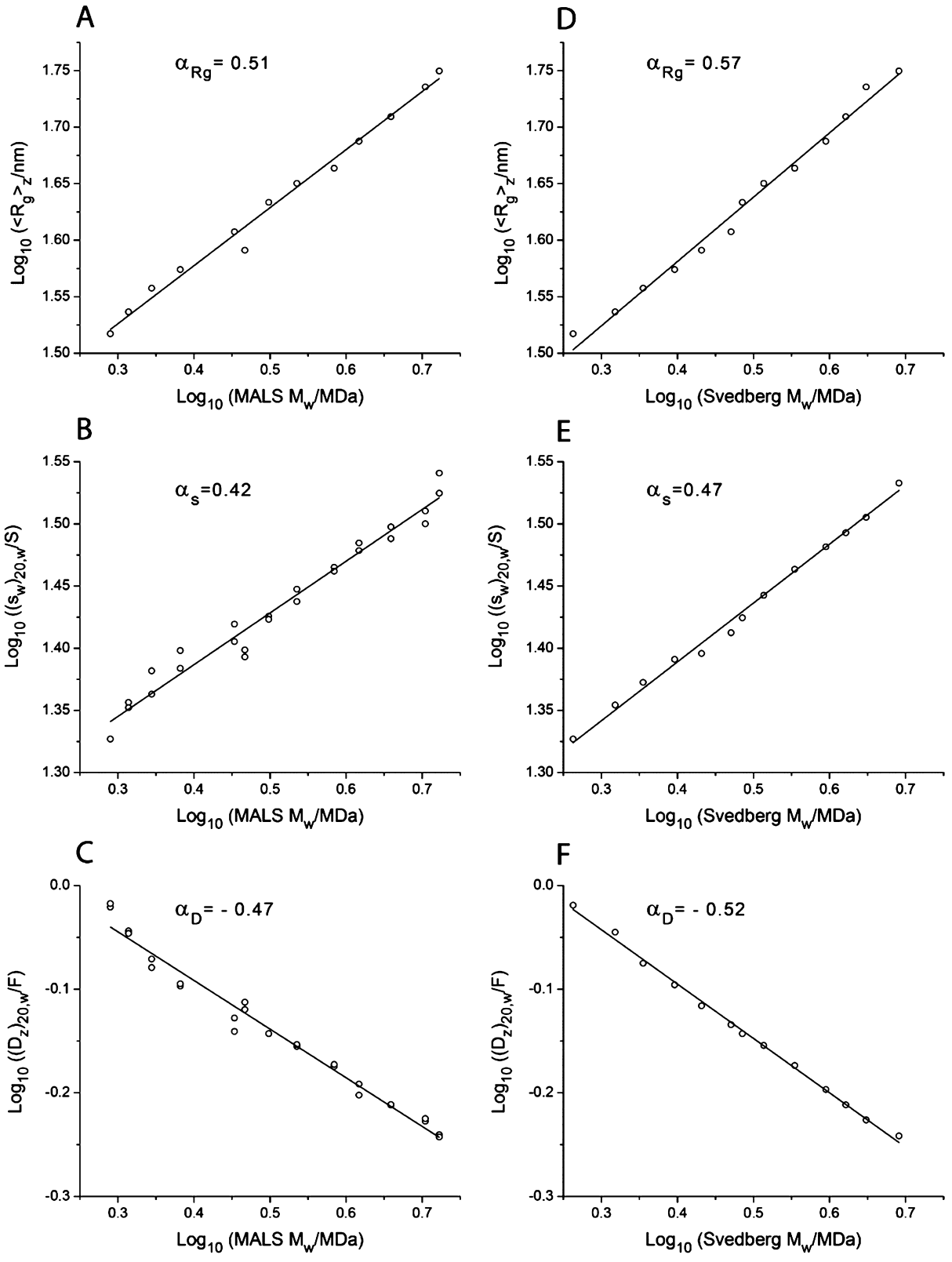

Figure 6. Conformation plots of SEC-fractionated VWF/fVIII complexes. Estimates of $\langle R_g \rangle_z$ and MALS M_w (Table 1), $\langle s_w \rangle_{20,w}$ (Table 2), $\langle D_z \rangle_{20,w}$ (Table 3), and Svedberg M_w (Table 4) for samples 1−13 of Sephacryl S-1000 -fractionated VWF/fVIII (Figure 1A) are plotted as $\log_{10} \langle R_g \rangle_z$, $\log_{10} (s_w)_{20,w}$, or $\log_{10} (D_z)_{20,w}$ vs $\log_{10}$ MALS M_w (A−C) or $\log_{10}$ Svedberg M_w (D−F). Also shown are the fitted regression lines and MHKS exponents obtained from the slopes of the regression lines.

of 70 and 2.5 nm for the contour length and diameter of the VWF subunit, respectively, estimated from electron microscopy,[16,61] yields a L/d ratio of 28. The a_G/a_T ratio corresponding to this value is 2.73. A bead model of the

https://doi.org/10.1021/acsomega.2c03389
ACS Omega 2022, 7, 31183−31196

Table 5. MHKS Exponents of Size-Fractionated VWF/fVIII Complexes[a]

	M_w estimate	
	MALS	Svedberg
α_{R_g}	0.51 ± 0.03	0.57 ± 0.05
α_s	0.42 ± 0.04	0.47 ± 0.03
α_D	−0.47 ± 0.03	−0.52 ± 0.03

[a]Means and 95% confidence intervals.

Table 6. MHKS Exponents for Defined Macromolecular Conformations[a]

MHKS exponent	sphere[d]	coil, no-EV[b,e]	coil, EV[c,e]	rod[d]
$\alpha_{R_g} = \alpha_{R_h} = \alpha_f$	0.33	0.5	0.6	1
α_s	0.67	0.5	0.4	0.15
α_D	−0.33	−0.5	−0.6	−0.85
$\alpha_{[\eta]}$	0	0.5	0.8	2

[a]EV: excluded volume. [b]Ideal random coil with no excluded volume or a real chain in a Θ-solvent. [c]Random coil with an excluded volume in a "good solvent". [d]References 23 and 24. [e]Reference22 Chapter XIV. $[\eta]$; Intrinsic viscosity.

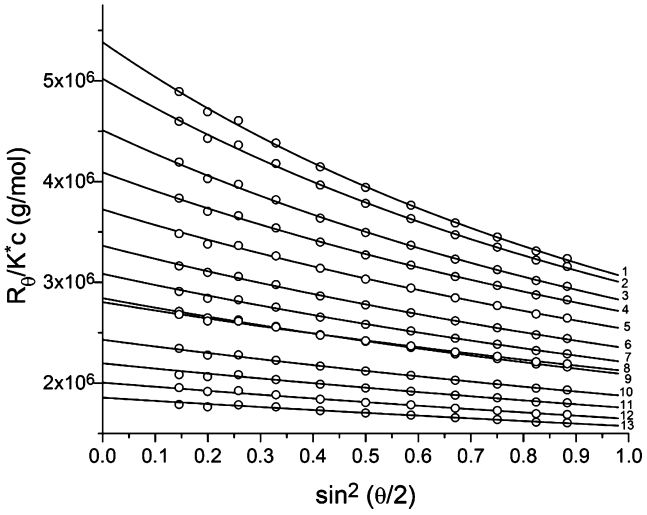

Figure 7. MALS random coil model of size-fractionated VWF/fVIII complexes. The data shown in Figure 2 representative of Superdex 200 SEC slices at the peak maxima for samples 1−13 of Sephacryl S-1000 -fractionated VWF/fVIII (Figure 1A) are replotted vs $\sin^2(\theta/2)$. The curves represent nonlinear least-squares regression fits to a random coil model (eq 7) using M_w and $(R_g)_z$ as the fitted parameters, as described in the Materials and Methods section.

wormlike chain has been developed, which produces the a_G/a_T ratio as a function of the L/P ratio and the diameter of the chain.[72] L/P ratios of 15 and 1090, which correspond to very stiff and very flexible wormlike chains, produce a_G/a_T ratios of 2.61 and 1.96, respectively.[24] Figure 8 shows the a_G/a_T ratio plotted as a function of M_w estimated using MALS or the Svedberg equation. The horizontal lines represent the a_G/a_T ratios for sphere, random coils, wormlike chains, and rods. The values cluster closely around the ratio expected for a random coil in the presence of an excluded volume.

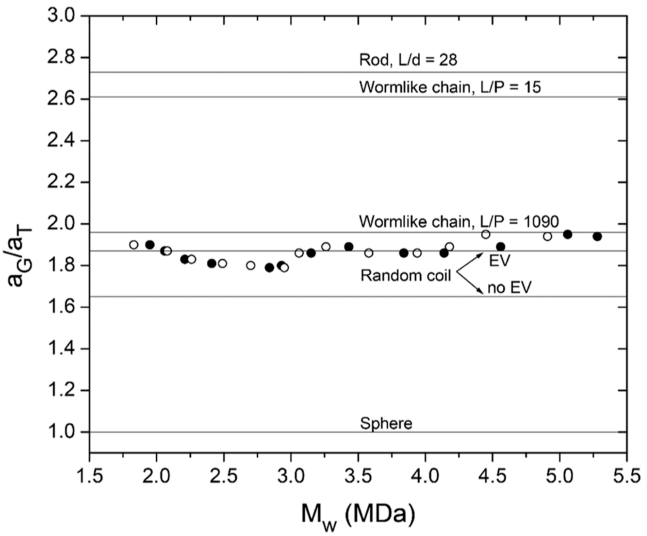

Figure 8. Ratios of equivalent radii, a_G/a_T, of size-fractionated VWF/fVIII complexes. The equivalent radii, a_G and a_T, for samples 1−13 of Sephacryl S-1000 -fractionated VWF/fVIII (Figure 1A) were calculated using the values of $\langle R_g \rangle_z$ and $(D_z)_{20,w}$ in Tables 1 and 3, respectively, as described in the Materials and Methods section. The dimensionless ratio, a_G/a_T, is plotted vs estimates of M_w obtained using MALS (closed circles) or the Svedberg equation (open circles). The horizontal lines correspond to a_G/a_T ratios for spheres, random coils, wormlike chains, and rods calculated as described in the Materials and Methods section. L/P, the ratio of contour length to persistence length; L/d, the ratio of rod length to diameter; and EV, excluded volume.

DISCUSSION

The results of this study are consistent with those of a random coil model of the VWF multimer under non-flowing conditions in which there is significant flexibility within the individual multimer subunits. For a homologous series of polymers such as a distribution of VWF multimers, conformation plots of the logarithmic relationship between molecular weight and the radius of gyration, the sedimentation coefficient, or the diffusion coefficient is used as a diagnostic for macromolecular conformation.[22−24] The slopes of the conformation plots produce the MHKS exponents, α_{R_g}, α_s, and α_D. Estimates of α_{R_g}, α_s, and α_D were all consistent with a random coil conformation of the VWF/fVIII multimer (Tables 5 and 6). These results do not support the widely held belief that the VWF multimer has a compact, globular conformation under static, non-flowing conditions.[14−19]

Although proteins can exhibit a random coil behavior under denaturing conditions,[73,74] VWF is an unusual example of a protein that exists as a random coil in its native conformation. Other examples include some members of the mucin family of glycoproteins.[75] Like VWF, mucins are heavily O-glycosylated and contain a cysteine-rich domain homologous to the VWF C and D domains, indicating a common evolutionary origin of the flexibility of these proteins.[76]

If characterized over sufficiently short lengths, a random coil is semi-flexible and exhibits some degree of stiffness. Most studies of the random coil behavior of macromolecules have been performed on synthetic polymers, polysaccharides, nucleic acids, or denatured proteins, in which the coil is defined in terms of repeating segments. In these macro-

https://doi.org/10.1021/acsomega.2c03389
ACS Omega 2022, 7, 31183−31196

molecules, the segment size is on the order of a few hundred daltons. The VWF/fVIII complex is an unusual example of a native protein displaying a random coil behavior. The segments of the VWF/fVIII coil evidently are ∼30−40 kDa subunit domains, which are much larger than the segments usually found in polymer chemistry. Additionally, there is extensive disulfide bonding between VWF subunits. Thus, it might be anticipated that some degree of stiffness in the VWF/fVIII complex would be readily apparent.

Semi-flexible macromolecules are usually modeled as a wormlike chain that has a conformation intermediate between a random coil and a rod.[20,24,72,77,78] The wormlike chain is similar to an elastic wire that bends smoothly along its length.[79] The stiffness of a wormlike chain is characterized by the relationship between its contour length, L, and persistence length, P.[24] In the coil limit, $L \gg P$, and in the rod limit, $L \ll P$ (ref 36, p 248), theoretical L/P ratios have been calculated as a function of the experimental ratio of equivalent radii, a_G/a_T.[72] The a_G/a_T ratios for VWF/fVIII complexes ranging from ∼2 to 5 MDa are all consistent with L/P ratios greater than 1000 (Figure 8). The contour length of the VWF subunit is ∼70 nm.[2] Thus, the persistence length is significantly shorter than the contour length of the VWF subunit. This indicates that the VWF subunit is very flexible and that domain−domain connections are freely jointed, which is the major conclusion of this study.

The segments of a random coil cannot overlap each other in space, which produces an excluded volume effect that tends to "swell" the coil and increase the radius of gyration. However, swelling reduces the number of available coil conformations, decreasing its entropy, which opposes swelling. Additionally, in "good solvents", segment−solvent interactions are more favorable than segment−segment interactions, which tends to expand the coil. Conversely, in "poor solvents", segment−solvent interactions are less favorable than segment−segment interactions, which tends to collapse the coil. The size of the coil, as measured by the radius of gyration, is a balance between excluded volume effects, conformational entropy, and segment−solvent interactions.

In the theoretical model of an ideal coil, the excluded volume restriction is removed.[22] For real coils, segment−segment interactions that are sufficiently favorable to reduce the size of the coil to its ideal limit produce an "unperturbed chain" (ref 22, p 423 ff; ref 36, p 241 ff). A solvent that produces these conditions is called a Θ-solvent. A model that remains in use for predicting MHKS exponents in good, poor and Θ-solvents was developed by Flory and co-workers over 70 years ago (Table 7).[22,24,80−83] Our estimates of the MHKS exponents lie between the Flory exponents predicted for a real chain in a good solvent subject to excluded volume effects and an unperturbed chain exhibiting segment−segment interactions (Table 7). This behavior is typical of synthetic polymers (ref 36, p 387) and proteins denatured in guanidine hydrochloride.[73] It has been proposed that this intermediate behavior is due to transient local ordering in a random coil.[74,84]

Table 7. Flory Scaling Relationships for a Random Coil

MHKS exponent	relationship to α_{R_g}
$\alpha_{R_g} = \alpha_{R_h} = \alpha_f$	—
α_s	$1 - \alpha_{R_g}$
α_D	$-\alpha_{R_g}$
$\alpha_{[\eta]}$	$3\alpha_{R_g} - 1$

Size-fractionated VWF/fVIII complexes are the possibly largest proteins whose molecular weights have been estimated by the first-principles physical methods of SV AUC/DLS and MALS. Although these methods have been used to characterize large DNA fragments, viruses, synthetic polymers, and other particles as large as or larger than VWF/fVIII complexes, possible differences of molecular weight estimates produced by the methods have not been frequently compared. Our results allowed an assessment of possible systematic errors in the two methods. In MALS, the instrument calibration factor, K^*, and the estimate of the macromolecular refractive index increment, dn/dc, along with a host of assumptions in the underlying theory,[37] are possible sources of systematic error. Additionally, the method requires extrapolation of light scattering intensities to zero angle to obtain the intercept and limiting slope that yield estimates of M_w and $\langle R_g \rangle_z$ (eq 1). The Berry[38] and Zimm[35,40] models are the most commonly used methods for this purpose. Light scattering data at both lower and higher angles can produce systematic errors, and there is no absolute method to determine which angles to include in the analysis.[39] We used angles ranging from 50 to 134° based on finding the optimum value of the coefficient of determination, r^2, from simple linear least-squares regression (see the Materials and Methods section). For the highest-molecular-weight multimers, the Zimm model produced estimates of $\langle R_g \rangle_z$ and M_w that were 12 and 4% higher, respectively, than those obtained using the Berry model (Table 1). These differences became progressively smaller with decreasing molecular weight. Andersson et al. have argued based on the analysis of simulated models that the Berry method is more accurate in the absence of a priori knowledge on the macromolecular structure,[39] and it was used for the subsequent analysis in our study.

Possible sources of errors in applying the Svedberg equation (eq 17) based on SV AUC/DLS measurements are systematic errors in the measurement of s_w, D_z, and partial specific volume. The Svedberg equation requires extrapolation of s_w and D_z to infinite dilution and to common solvent conditions, typically water at 20 °C, producing $(s_w^0)_{20,w}$ and $(D_z^0)_{20,w}$, respectively. For unfractionated VWF/fVIII complexes, s_w values decrease by ∼20% at 1 mg/mL from the value extrapolated to infinite dilution.[25] To decrease this source of error while retaining an adequate signal, SV AUC measurements were obtained using a nominal loading concentration of 0.15 mg/mL (Figure 3A). The conversion of the DLS decay rate to a diffusion coefficient (eq 12) assumes that the diffusing particles are small relative to the incident wavelength of light. Because the estimates of the hydrodynamic radii of the VWF/fVIII multimers ranged from 22 to 37 nm (Table 4) compared to the 633 nm wavelength of incident of DLS light, we assume that this assumption is valid. Dust and other large particle contaminants and the angular dependence of scattering are also a potential source of systematic error in DLS measurements. The partial specific volume appears in the denominator of the Svedberg equation as $1 - \bar{\nu}\rho$. Thus, small errors in its estimation can produce significant errors in the estimate of M_w. For example, increasing the partial specific volume estimate for VWF from the value estimated from the amino acid and

https://doi.org/10.1021/acsomega.2c03389
ACS Omega 2022, 7, 31183−31196

carbohydrate composition, 0.706, to 0.72 mL/g decreases the molecular weight by 5%.

The M_w estimates of SEC-fractionated VWF/fVIII complexes by MALS and using the Svedberg equation were compared using Bland—Altman analysis[67] (Figure 5B). There was a bias toward MALS estimates producing higher estimates, which was more pronounced at higher molecular weights. However, the estimates were within 4% on average, indicating the good agreement between the two methods.

Slayter et al. performed DLS and MALS measurements on plasma-derived human VWF fractionated by Sephacryl S-1000 SEC and reported R_h values ranging from 58 to 86 nm and R_g values ranging from 92 to 130 nm.[14] These values are larger than the highest values we measured (Tables 1 and 4). The reason for this difference is not clear. Slayter et al. did not describe which fractions were selected for analysis or report molecular weight estimates of the fractions, which may have been higher than the fractions selected for our study. The VWF/fVIII complexes sampled in our study are physiologically relevant because they represent the bulk of the population present in a therapeutic VWF/fVIII product (Figure 1).

In summary, conformation plots of size-fractionated VWF/fVIII complexes with molecular weights ranging from ∼2 to 5 MDa independently estimated by SV AUC/DLS and MALS are consistent with a random coil conformation. Ratios of radii of gyration to hydrodynamic radii of the complexes indicate that the persistence length is significantly shorter than the contour length of the VWF subunit, consistent with a high degree of flexibility between the domains of the VWF subunit.

■ ASSOCIATED CONTENT

Supporting Information

The Supporting Information is available free of charge at https://pubs.acs.org/doi/10.1021/acsomega.2c03389.

Angle selection for MALS analysis, concentration dependence of $(D_z)_{20,w}$ values, Berry plot of sample 9, and $(D_z)_{20,w}$ estimates of SEC-fractionated VWF/fVIII complexes (PDF)

Accession Codes

Accession Codes: Von Willebrand factor: P04275. Factor VIII: P00451.

■ AUTHOR INFORMATION

Corresponding Author

Pete Lollar − *Aflac Cancer and Blood Disorders Center, Children's Healthcare of Atlanta; Department of Pediatrics, Emory University, Atlanta, Georgia 30322, United States;* orcid.org/0000-0002-1206-8104; Email: jlollar@emory.edu

Authors

Ernest T. Parker − *Aflac Cancer and Blood Disorders Center, Children's Healthcare of Atlanta; Department of Pediatrics, Emory University, Atlanta, Georgia 30322, United States*

Sandra L. Haberichter − *Diagnostic Laboratories and Blood Research Institute, Versiti, Milwaukee, Wisconsin 53201-2178, United States; Pediatric Hematology/Oncology, Medical College of Wisconsin, Milwaukee, Wisconsin 53226, United States; Children's Research Institute, Children's Hospital of Wisconsin, Milwaukee, Wisconsin 53226, United States*

Complete contact information is available at: https://pubs.acs.org/10.1021/acsomega.2c03389

Author Contributions

The manuscript was written through contributions of all authors. All authors have given approval to the final version of the manuscript.

Funding

This work was supported by the National Institutes of Health/National Heart, Lung, and Blood Institute (award number U54HL141981 to P.L and award numbers R01 HL136430 and P01 144457 to S.L.H.). The content is solely the responsibility of the authors and does not necessarily represent the official views of the National Institutes of Health.

Notes

The authors declare no competing financial interest.

■ ABBREVIATIONS

VWF, von Willebrand factor; fVIII, factor VIII; DLS, dynamic light scattering; SV AUC, sedimentation velocity analytical ultracentrifugation; SEC, size-exclusion chromatography; MALS, multi-angle light scattering; MHKS, Mark−Houwink−Kuhn−Sakurada; HBSCa, 0.15 M NaCl, 0.02 M Hepes, 5 mM $CaCl_2$, pH 7.4

■ REFERENCES

(1) Sadler, J. E. Biochemistry and genetics of von Willebrand factor. *Annu. Rev. Biochem.* **1998**, *67*, 395−424.

(2) Springer, T. A. von Willebrand factor, Jedi knight of the bloodstream. *Blood* **2014**, *124*, 1412.

(3) Johnsen, J.; Ginsburg, D. von Willebrand Disease. In *Williams Hematology*, 9th ed.; Kaushansky, K., Lichtman, M. A., Prchal, J. T., Levi, M. M., Press, O. M., Burns, L. J., Caligiuri, M. A., Eds.: McGraw Hill: New York, 2016; pp 2163−2182.

(4) Chopek, M. W.; Girma, J. P.; Fujikawa, K.; Davie, E. W.; Titani, K. Human von Willebrand factor: a multivalent protein composed of identical subunits. *Biochemistry* **1986**, *25*, 3146−3155.

(5) Titani, K.; Kumar, S.; Takio, K.; Ericsson, L. H.; Wade, R. D.; Ashida, K.; Walsh, K. A.; Chopek, M. W.; Sadler, J. E.; Fujikawa, K. Amino acid sequence of human von Willebrand factor. *Biochemistry* **1986**, *25*, 3171−3184.

(6) Dong, X. C.; Leksa, N. C.; Chhabra, E. S.; Arndt, J. W.; Lu, Q.; Knockenhauer, K. E.; Peters, R. T.; Springer, T. A. The von Willebrand factor D ' D3 assembly and structural principles for factor VIII binding and concatemer biogenesis. *Blood* **2019**, *133*, 1523−1533.

(7) Emsley, J.; Cruz, M.; Handin, R.; Liddington, R. Crystal structure of the von Willebrand factor A1 domain and implications for the binding of platelet glycoprotein Ib. *J. Biol. Chem.* **1998**, *273*, 10396−10401.

(8) Zhang, Q.; Zhou, Y. F.; Zhang, C. Z.; Zhang, X. H.; Lu, C. F.; Springer, T. A. Structural specializations of A2, a force-sensing domain in the ultralarge vascular protein von Willebrand factor. *Proc. Natl. Acad. Sci. U.S.A.* **2009**, *106*, 9226−9231.

(9) Bienkowska, J.; Cruz, M.; Atiemo, A.; Handin, R.; Liddington, R. The von Willebrand factor A3 domain does not contain a metal ion-dependent adhesion site motif. *J. Biol. Chem.* **1997**, *272*, 25162−25167.

(10) Ruggeri, Z. M.; Zimmerman, T. S. Variant von Willebrand's disease: Characterization of 2 subtypes by analysis of multimeric composition of factor VIII/von Willebrand factor in plasma and platelets. *J. Clin. Invest.* **1980**, *65*, 1318−1325.

(11) Sadler, J. E.; Sadler, J. E. von Willebrand factor assembly and secretion. *J. Thromb. Haemostasis* **2009**, *7*, 24−27.

(12) Moake, J. L.; Rudy, C. K.; Troll, J. H.; Weinstein, M. J.; Colannino, N. M.; Azocar, J.; Seder, R. H.; Hong, S. L.; Deykin, D. Unusually large plasma factor VIII - von Willebrand factor multimers

in chronic relapsing thrombotic thrombocytopenic purpura. *N. Engl. J. Med.* **1982**, *307*, 1432−1435.
(13) Levy, G. G.; Nichols, W. C.; Lian, E. C.; Foroud, T.; McClintick, J. N.; McGee, B. M.; Yang, A. Y.; Siemieniak, D. R.; Stark, K. R.; Gruppo, R.; Sarode, R.; Shurin, S. B.; Chandrasekaran, V.; Stabler, S. P.; Sabio, H.; Bouhassira, E. E.; Upshaw, J. D.; Ginsburg, D.; Tsai, H. M. Mutations in a member of the ADAMTS gene family cause thrombotic thrombocytopenic purpura. *Nature* **2001**, *413*, 488−494.
(14) Slayter, H.; Loscalzo, J.; Bockenstedt, P.; Handin, R. I. Native conformation of human von Willebrand protein. Analysis by electron microscopy and quasi-elastic light scattering. *J. Biol. Chem.* **1985**, *260*, 8559−8563.
(15) Fowler, W. E.; Fretto, L. J.; Hamilton, K. K.; Erickson, H. P.; McKee, P. A. Substructure of human von Willebrand factor. *J. Clin. Invest.* **1985**, *76*, 1491−1500.
(16) Zhou, Y. F.; Eng, E. T.; Nishida, N.; Lu, C. F.; Walz, T.; Springer, T. A. A pH-regulated dimeric bouquet in the structure of von Willebrand factor. *EMBO J.* **2011**, *30*, 4098−4111.
(17) Springer, T. A. Biology and physics of von Willebrand factor concatamers. *J. Thromb. Haemostasis* **2011**, *9*, 130−143.
(18) Sing, C. E.; Alexander-Katz, A. Elongational flow induces the unfolding of von Willebrand factor at physiological flow rates. *Biophys. J.* **2010**, *98*, L35−L37.
(19) Fu, H. X.; Jiang, Y.; Yang, D. R.; Scheiflinger, F.; Wong, W. P.; Springer, T. A. Flow-induced elongation of von Willebrand factor precedes tension-dependent activation. *Nat. Commun.* **2017**, *8*, 324.
(20) Hiemenz, P. C.; Lodge, T. P. *Polymer Chemistry*. 2nd ed.; CRC Press: Boca Raton, 2007.
(21) Rubinstein, M.; Colby, R. H. *Polymer Physics*; Oxford University Press: Oxford, 2003.
(22) Flory, P. J. *Principles of Polymer Chemistry*; Cornell University Press: Ithaca, 1953.
(23) Gillis, R. B.; Rowe, A. J.; Adams, G. G.; Harding, S. E. A review of modern approaches to the hydrodynamic characterisation of polydisperse macromolecular systems in biotechnology. *Biotechnol. Genet. Eng. Rev.* **2014**, *30*, 142−157.
(24) García de la Torre, J.; Hernández Cifre, J. G. H. Hydrodynamic properties of biomacromolecules and macromolecular complexes: concepts and methods. A tutorial mini-review. *J. Mol. Biol.* **2020**, *432*, 2930−2948.
(25) Parker, E. T.; Lollar, P. Conformation of the von Willebrand factor/factor VIII complex in quasi-static flow. *J. Biol. Chem.* **2021**, *296*, 100420.
(26) Mannucci, P. M.; Chediak, J.; Hanna, W.; Byrnes, J.; Ledford, M.; Ewenstein, B. M.; Retzios, A. D.; Kapelan, B. A.; Schwartz, R. S.; Kessler, C.; Alphanate Study, G. Treatment of von Willebrand disease with a high-purity factor VIII/von Willebrand factor concentrate: a prospective, multicenter study. *Blood* **2002**, *99*, 450−456.
(27) Santagostino, E. More than a decade of international experience with a pdFVIII/VWF concentrate in immune tolerance. *Haemophilia* **2013**, *19*, 8−11.
(28) Pace, C. N.; Vajdos, F.; Fee, L.; Grimsley, G.; Gray, T. How to measure and predict the molar absorption coefficient of a protein. *Protein Sci.* **1995**, *4*, 2411−2423.
(29) Cohn, E. J.; Edsall, J. T. Density and apparent specific volume of proteins. In *Proteins, Amino-Acids and Peptides as Dipolar Ions*; Cohn, E. J., Edsall, J. T., Eds.; Van Nostrand-Reinhold: Princeton, 1943.
(30) Zhao, H.; Brown, P. H.; Schuck, P. On the distribution of protein refractive index increments. *Biophys. J.* **2011**, *100*, 2309−2317.
(31) Cole, J. L.; Lary, J. W.; Moody, P. M.; Laue, T. M. Analytical ultracentrifugation: sedimentation velocity and sedimentation equilibrium. *Methods Cell Biol.* **2008**, *84*, 143−179.
(32) Schuck, P.; Zhao, H.; Brautigam, C. A.; Ghirlando, R. *Basic Principles of Analytical Ultracentrifugation*; CRC Press: Boca Raton, 2016.
(33) Doering, C. B.; Healey, J. F.; Parker, E. T.; Barrow, R. T.; Lollar, P. Identification of porcine coagulation factor VIII domains responsible for high level expression via enhanced secretion. *J. Biol. Chem.* **2004**, *279*, 6546−6552.
(34) Flood, V. H.; Gill, J. C.; Friedman, K. D.; Christopherson, P. A.; Jacobi, P. M.; Hoffmann, R. G.; Montgomery, R. R.; Haberichter, S. L.; Zimmerman Program, I. Collagen binding provides a sensitive screen for variant von Willebrand disease. *Clin. Chem.* **2013**, *59*, 684−691.
(35) Wyatt, P. J. Light scattering and the absolute characterization of macromolecules. *Anal. Chim. Acta* **1993**, *272*, 1−40.
(36) Lodge, T. P.; Hiemenz, P. C., *Polymer Chemistry*. 3rd ed.; CRC Press: Boca Raton, 2020.
(37) Tanford, C. *Physical Chemistry of Macromolecules*; John Wiley & Sons: New York, 1961.
(38) Berry, G. C. Thermodynamic and conformational properties of polystyrene. I. Light-scattering studies on dilute solutions of linear polystyrenes. *J. Chem. Phys.* **1966**, *44*, 4550−4564.
(39) Andersson, M.; Wittgren, B.; Wahlund, K. G. Accuracy in multiangle light scattering measurements for molar mass and radius estimations. Model calculations and experiments. *Anal. Chem.* **2003**, *75*, 4279−4291.
(40) Zimm, B. H. The scattering of light and radial distribution function of high polymer solutions. *J. Chem. Phys.* **1948**, *16*, 1093−1099.
(41) Debye, P. Molecular-weight determination by light scattering. *J. Phys. Colloid Chem.* **1947**, *51*, 18−32.
(42) Zhao, H.; Brautigam, C. A.; Ghirlando, R.; Schuck, P. Overview of current methods in sedimentation velocity and sedimentation equilibrium analytical ultracentrifugation. *Curr. Protoc. Protein Sci.* **2013**, *20*, Unit20.
(43) Ghirlando, R.; Zhao, H.; Balbo, A.; Piszczek, G.; Curth, U.; Brautigam, C. A.; Schuck, P. Measurement of the temperature of the resting rotor in analytical ultracentrifugation. *Anal. Biochem.* **2014**, *458*, 37−39.
(44) Zhao, H.; Ghirlando, R.; Alfonso, C.; Arisaka, F.; Attali, I.; Bain, D. L.; Bakhtina, M. M.; Becker, D. F.; Bedwell, G. J.; Bekdemir, A.; Besong, T. M.; Birck, C.; Brautigam, C. A.; Brennerman, W.; Byron, O.; Bzowska, A.; Chaires, J. B.; Chaton, C. T.; Cölfen, H.; Connaghan, K. D.; Crowley, K. A.; Curth, U.; Daviter, T.; Dean, W. L.; Díez, A. I.; Ebel, C.; Eckert, D. M.; Eisele, L. E.; Eisenstein, E.; England, P.; Escalante, C.; Fagan, J. A.; Fairman, R.; Finn, R. M.; Fischle, W.; de la Torre, J. G.; Gor, J.; Gustafsson, H.; Hall, D.; Harding, S. E.; Cifre, J. G.; Herr, A. B.; Howell, E. E.; Isaac, R. S.; Jao, S. C.; Jose, D.; Kim, S. J.; Kokona, B.; Kornblatt, J. A.; Kosek, D.; Krayukhina, E.; Krzizike, D.; Kusznir, E. A.; Kwon, H.; Larson, A.; Laue, T. M.; Le Roy, A.; Leech, A. P.; Lilie, H.; Luger, K.; Luque-Ortega, J. R.; Ma, J.; May, C. A.; Maynard, E. L.; Modrak-Wojcik, A.; Mok, Y. F.; Mücke, N.; Nagel-Steger, L.; Narlikar, G. J.; Noda, M.; Nourse, A.; Obsil, T.; Park, C. K.; Park, J. K.; Pawelek, P. D.; Perdue, E. E.; Perkins, S. J.; Perugini, M. A.; Peterson, C. L.; Peverelli, M. G.; Piszczek, G.; Prag, G.; Prevelige, P. E.; Raynal, B. D.; Rezabkova, L.; Richter, K.; Ringel, A. E.; Rosenberg, R.; Rowe, A. J.; Rufer, A. C.; Scott, D. J.; Seravalli, J. G.; Solovyova, A. S.; Song, R.; Staunton, D.; Stoddard, C.; Stott, K.; Strauss, H. M.; Streicher, W. W.; Sumida, J. P.; Swygert, S. G.; Szczepanowski, R. H.; Tessmer, I.; Toth, R. T. t.; Tripathy, A.; Uchiyama, S.; Uebel, S. F.; Unzai, S.; Gruber, A. V.; von Hippel, P. H.; Wandrey, C.; Wang, S. H.; Weitzel, S. E.; Wielgus-Kutrowska, B.; Wolberger, C.; Wolff, M.; Wright, E.; Wu, Y. S.; Wubben, J. M.; Schuck, P. A multilaboratory comparison of calibration accuracy and the performance of external references in analytical ultracentrifugation. *PLoS One* **2015**, *10*, No. e0126420.
(45) Schuck, P. Size-distribution analysis of macromolecules by sedimentation velocity ultracentrifugation and Lamm equation modeling. *Biophys. J.* **2000**, *78*, 1606−1619.
(46) Dam, J.; Schuck, P. Calculating sedimentation coefficient distributions by direct modeling of sedimentation velocity concentration profiles. *Methods Enzymol.* **2004**, *384*, 185−212.
(47) Schuck, P. *Sedimentation Velocity Analytical Ultracentrifugation*; CRC Press: Boca Raton, 2017.

https://doi.org/10.1021/acsomega.2c03389
ACS Omega 2022, 7, 31183−31196

(48) Brautigam, C. A. Calculations and publication-quality illustrations for analytical ultracentrifugation data. *Methods Enzymol.* **2015**, *562*, 109−133.
(49) Schachman, H. K. *Ultracentrifugation in Biochemistry*; Academic Press: New York, 1959.
(50) Schuck, P. On the analysis of protein self-association by sedimentation velocity analytical ultracentrifugation. *Anal. Biochem.* **2003**, *320*, 104−124.
(51) Frisken, B. J. Revisiting the method of cumulants for the analysis of dynamic light-scattering data. *Appl. Opt.* **2001**, *40*, 4087−4091.
(52) Koppel, D. E. Analysis of macromolecular polydispersity in intensity correlation spectroscopy - method of cumulants. *J. Chem. Phys.* **1972**, *57*, 4814−4820.
(53) Parker, E. T.; Lollar, P. Measurement of the translational diffusion coefficient and hydrodynamic radius of proteins by dynamic light scattering. *Bio-Protoc.* **2021**, *11*, No. e4195.
(54) Cantor, C. R.; Schimmel, P. R. Size and shape of macromolecules. *Biophysical Chemistry. Part II. Techniques for the Study of Biological Structure and Function*; W.H. Freeman and Co.: San Francisco, 1980; pp 539−590.
(55) Brautigam, C. A. Applications and complementarity of analytical ultracentrifugation and light scattering. In *Biomolecular and Bioanalytical Techniques*; Ramesh, V., Ed.; John Wiley & Sons: Hoboken, 2019; pp 255−278. DOI: 10.1002/9781119483977.ch11
(56) Cantor, C. R.; Schimmel, P. R. Ultracentrifugation. *Biophysical Chemistry. Part II. Techniques for the Study of Biological Structure and Function*; W.H. Freeman and Co.: San Francisco, 1980; pp 591−642.
(57) Kinell, P. O. On the determination of molecular weight averages from sedimentation and diffusion data. *Ark. Kemi* **1959**, *14*, 327−336.
(58) Stetefeld, J.; McKenna, S. A.; Patel, T. R. Dynamic light scattering: a practical guide and applications in biomedical sciences. *Biophys. Rev.* **2016**, *8*, 409−427.
(59) Einstein, A. E. *Investigations on the Theory of Brownian Movement*; Methuen Co. & Dover Publications: New York, 1926.
(60) Ortega, A.; García de la Torre, J. Equivalent radii and ratios of radii from solution properties as indicators of macromolecular conformation, shape, and flexibility. *Biomacromolecules* **2007**, *8*, 2464−2475.
(61) Ohmori, K.; Fretto, L. J.; Harrison, R. L.; Switzer, M. E.; Erickson, H. P.; McKee, P. A. Electron microscopy of human factor VIII/Von Willebrand glycoprotein: effect of reducing reagents on structure and function. *J. Cell Biol.* **1982**, *95*, 632−640.
(62) Ortega, A.; García de la Torre, J. G. Hydrodynamic properties of rodlike and disklike particles in dilute solution. *J. Chem. Phys.* **2003**, *119*, 9914−9919.
(63) Tellinghuisen, J. Least Squares Methods for Treating Problems with Uncertainty in x and y. *Anal. Chem.* **2020**, *92*, 10863−10871.
(64) Linnet, K. Estimation of the linear relationships between the measurements of 2 methods with proportional errors. *Stat. Med.* **1990**, *9*, 1463−1473.
(65) Lebowitz, J.; Lewis, M. S.; Schuck, P. Modern analytical ultracentrifugation in protein science: a tutorial review. *Protein Sci.* **2002**, *11*, 2067−2079.
(66) Oncley, J. L. Evidence from physical chemistry regarding the size and shape of protein molecules from ultracentrifugation, diffusion, viscosity, dielectric dispersion, and double refraction of flow. *Ann. N.Y. Acad. Sci.* **1941**, *41*, 121−150.
(67) Altman, D. G.; Bland, J. M. Measurement in medicine - the analysis of method comparison studies. *J. R. Stat. Soc.—Ser. D Statistician* **1983**, *32*, 307−317.
(68) Zaccai, N. R.; Serdyuk, I. N.; Zaccai, J., Hydrodynamics. In *Methods in Molecular Biophysics*, 2nd ed.; Cambridge University Press: Cambridge, 2017; pp 159−250.
(69) Garcia De la Torre, J.; Lopez Martinez, M. C. L.; Tirado, M. M.; Freire, J. J. Monte Carlo study of hydrodynamic properties of flexible linear chains: analysis of several approximate methods. *Macromolecules* **1984**, *17*, 2715−2722.
(70) Freire, J. J.; Rey, A.; Garcia de la Torre, J. Monte Carlo calculations for linear and star polymers with intramolecular interactions. 2. Non-preaveraged study of hydrodynamic properties at the theta state. *Macromolecules* **1986**, *19*, 457−462.
(71) Garcia Bernal, J. M.; Tirado, M. M.; Freire, J. J.; Garcia de la Torre, J. Monte Carlo calculation of hydrodynamic properties of linear and cyclic polymers in good solvents. *Macromolecules* **1991**, *24*, 593−598.
(72) Amorós, D.; Ortega, A.; García de la Torre, J. Hydrodynamic properties of wormlike macromolecules: Monte Carlo simulation and global analysis of experimental data. *Macromolecules* **2011**, *44*, 5788−5797.
(73) Tanford, C.; Kawahara, K.; Lapanje, S. Proteins as random coils. I. Intrinsic viscosities and sedimentation coefficients in concentrated guanidine hydrochloride. *J. Am. Chem. Soc.* **1967**, *89*, 729−736.
(74) Baldwin, R. L.; Zimm, B. H. Are denatured proteins ever random coils? *Proc. Natl. Acad. Sci. U.S.A.* **2000**, *97*, 12391−12392.
(75) Harding, S. E.; Abdelhameed, A. S.; Morris, G. A. On the hydrodynamic analysis of conformation in mixed biopolymer systems. *Polym. Int.* **2011**, *60*, 2−8.
(76) Javitt, G.; Khmelnitsky, L.; Albert, L.; Bigman, L. S.; Elad, N.; Morgenstern, D.; Ilani, T.; Levy, Y.; Diskin, R.; Fass, D. Assembly mechanism of mucin and von Willebrand factor polymers. *Cell* **2020**, *183*, 717−729.
(77) Kratky, O.; Porod, G. Rontgenuntersuchung geloster fadenmolekule. *Recl. Trav. Chim. Pays-Bas* **1949**, *68*, 1106−1122.
(78) Yamakawa, H.; Fujii, M. Translational friction coefficient of wormlike chains. *Macromolecules* **1973**, *6*, 407−415.
(79) García Molina, J. J.; García de la Torre, J. The randomly broken chain as a semiflexible macromolecular model - computer simulation of statistical properties. *J. Chem. Phys.* **1986**, *84*, 4026−4030.
(80) Flory, P. J. The configuration of real polymer chains. *J. Chem. Phys.* **1949**, *17*, 303−310.
(81) Flory, P. J.; Fox, T. G. Treatment of intrinsic viscosities. *J. Am. Chem. Soc.* **1951**, *73*, 1904−1908.
(82) Krigbaum, W. R.; Mandelkern, L.; Flory, P. J. Molecular weight dependence of intrinsic viscosity of polymer solutions. *J. Polym. Sci.* **1952**, *9*, 381−384.
(83) Mandelkern, L.; Flory, P. J. The frictional coefficient for flexible chain molecules in dilute solution. *J. Chem. Phys.* **1952**, *20*, 212−214.
(84) Berry, G. C. The hydrodynamic and conformational properties of denatured proteins in dilute solutions. *Protein Sci.* **2010**, *19*, 94−98.

https://doi.org/10.1021/acsomega.2c03389
ACS Omega 2022, 7, 31183−31196